

## Accepted Manuscript

Longshore wave energy flux: Variability and trends in the southern coast of Buenos Aires, Argentina

Iael Pérez, Guadalupe Alonso, Andrés Pescio, Walter Dragani, Jorge Codignotto



PII: S2352-4855(16)30258-4  
DOI: <http://dx.doi.org/10.1016/j.rsma.2017.08.002>  
Reference: RSMA 269

To appear in: *Regional Studies in Marine Science*

Received date: 7 November 2016  
Revised date: 3 August 2017  
Accepted date: 3 August 2017

Please cite this article as: Pérez I., Alonso G., Pescio A., Dragani W., Codignotto J., Longshore wave energy flux: Variability and trends in the southern coast of Buenos Aires, Argentina. *Regional Studies in Marine Science* (2017), <http://dx.doi.org/10.1016/j.rsma.2017.08.002>

This is a PDF file of an unedited manuscript that has been accepted for publication. As a service to our customers we are providing this early version of the manuscript. The manuscript will undergo copyediting, typesetting, and review of the resulting proof before it is published in its final form. Please note that during the production process errors may be discovered which could affect the content, and all legal disclaimers that apply to the journal pertain.

**Longshore wave energy flux: variability and trends in the southern coast of Buenos Aires, Argentina**

Iael Pérez<sup>1,2,\*</sup>, Guadalupe Alonso<sup>1,3</sup>, Andrés Pescio<sup>1,3</sup>, Walter Dragani<sup>1,2,3,4</sup> and Jorge Codignotto<sup>2,5</sup>

<sup>(1)</sup> Servicio de Hidrografía Naval, Av. Montes de Oca 2124 (C1270ABV) Ciudad Autónoma de Buenos Aires, Argentina

<sup>(2)</sup> CONICET, Consejo Nacional de Investigaciones Científicas y Técnicas. Av. Rivadavia 1917. (C1033AAJ) Ciudad Autónoma de Buenos Aires, Argentina

<sup>(3)</sup> Departamento de Ciencias de la Atmósfera y los Océanos, Facultad de Ciencias Exactas y Naturales, UBA, Ciudad Universitaria, Pabellón II, 2do. Piso. (C1428EGA) Ciudad Autónoma de Buenos Aires, Argentina

<sup>(4)</sup> Instituto Franco-Argentino para el Estudio del Clima y sus Impactos (UMI IFAECI/CNRS-CONICET-UBA), Ciudad Universitaria, Pabellón II, 2do. Piso. (C1428EGA) Ciudad Autónoma de Buenos Aires, Argentina

<sup>(5)</sup> Servicio Geológico Minero Argentino (SEGEMAR), Av. Julio A. Roca 651 101 P (C1067ABB), Ciudad Autónoma de Buenos Aires, Argentina

\* Corresponding author [iaelperez@gmail.com](mailto:iaelperez@gmail.com), Servicio de Hidrografía Naval, Av. Montes de Oca 2124 (C1270ABV)

Revised manuscript submitted to Regional Studies in Marine Science

August, 2017

**Abstract:** Variability and trends of the longshore wave energy flux were analyzed between Bahía Blanca and Mar del Plata, along the southern coast of Buenos Aires, Argentina. Longshore energy flux was assessed from wave parameters obtained from long-term numerical simulations carried out with a validated model (Simulated Waves Nearshore model) for the period 1979-2012. It was determined that the longshore energy flux flows predominantly eastwards. Mean values and standard deviations of the longshore flux increased eastwards. Two different areas were defined in the study region: the eastern area, characterized by higher values of longshore energy flux, and the western one, where fluxes were approximately 14% of the eastern values. Longshore wave energy flux did not present significant long term trends in the study region. High inter-annual variability in longshore wave energy flux was observed especially at the eastern area of the study region. Possible connections between this inter-annual variability and climatic indices related to El Niño / Southern Oscillation and the Southern Annual Oscillation were investigated. Significant correlation coefficients were obtained for both indices at the easternmost locations of the study region. This indicates that both climatic anomalies can impact on the wave climate and littoral processes along the southern coast of Buenos Aires.

**Keywords:** waves; longshore energy flux; climatic variability; trends; southern coast of Buenos Aires; climatic indices

## 1. Introduction

Every coastal management strategy requires, among other issues, adequate information about the wave climate (Delgado et al., 2012). Waves are an essential factor in the hydrodynamic and geomorphology of coastal regions, particularly on sandy beaches. This phenomenon not only suspends the sediments but also triggers nearshore currents that carry the suspended sediments along or across-shore (Dean and Dalrymple, 2002). Several works showed evident changes in the wind wave climate from a global and regional perspective. One of the global studies was

60  
61  
62 carried out by Young et al. (2011) by means of 23 years of validated and calibrated altimeter  
63 data. They found a clear significant trend of increasing extreme wave height at high latitudes  
64 and more neutral conditions in equatorial regions. Moreover, using results from a community  
65 derived multi-model ensemble of wave-climate projections Hemer et al. (2013) found an  
66 increase in annual mean significant wave height over 7.1 % of the global ocean, predominantly  
67 in the Southern Ocean, which is greater during austral winter (July–September; 8.8%). Within  
68 more regional studies, in the North Atlantic Ocean over the 20th century a significant increase  
69 in wave height was reported by Bertin et al. (2013), who developed a 109 year numerical wind-  
70 wave hindcast. For Latin America and the Caribbean region, Reguero et al. (2013) described  
71 the wave climatology based on the global wave reanalysis forced with the reanalysis from the  
72 National Center for Environmental Prediction / National Center for Atmospheric Research  
73 (NCEP/NCAR, Kalnay et al., 1996). Long-term changes were identified in the wave heights  
74 and mean direction of the energy flux, which showed high space variability. Finally, space and  
75 time variability of extreme wave climate was analyzed by Izaguirre et al. (2013).  
76  
77  
78  
79  
80  
81  
82  
83  
84  
85  
86  
87  
88  
89  
90  
91  
92  
93  
94  
95  
96  
97  
98  
99  
100  
101  
102  
103  
104  
105  
106  
107  
108  
109  
110  
111  
112  
113  
114  
115  
116  
117  
118

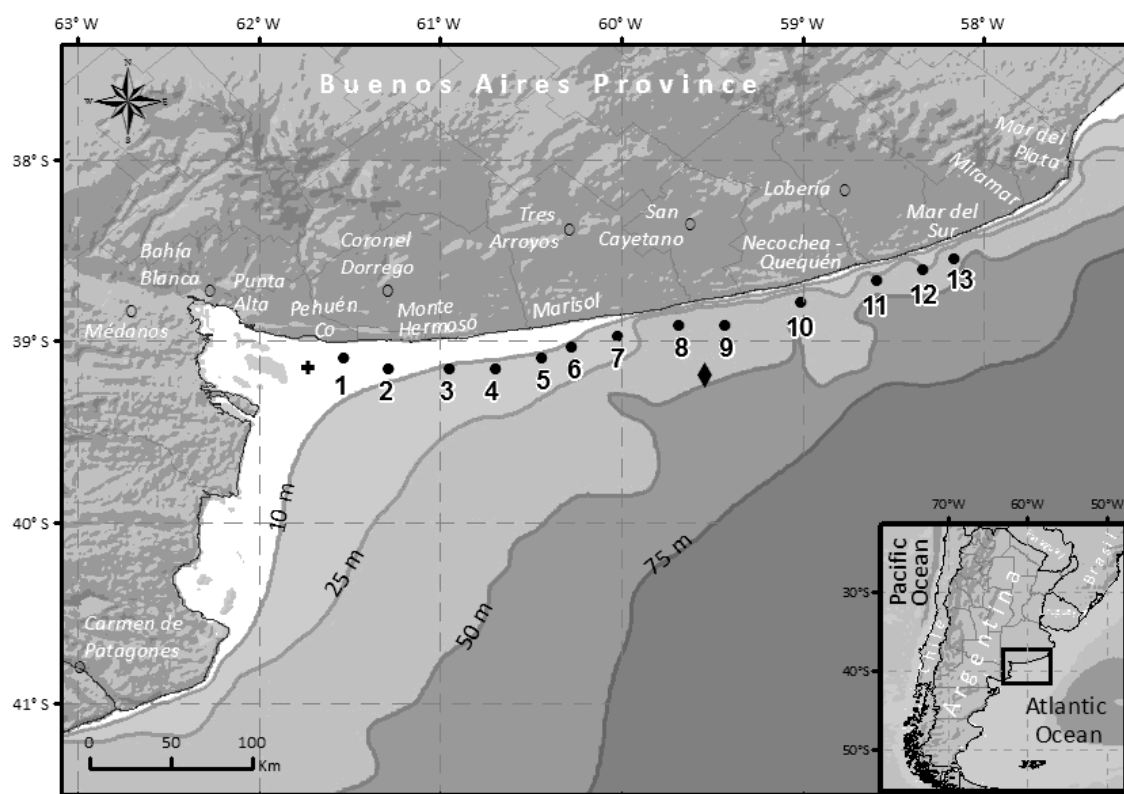


**Figure 1.** The southern coast of Buenos Aires (Argentina) and its locations, in the southwestern Atlantic Ocean.

Numbers indicate the position of the analyzed locations. The black cross indicates the position of the wave gauge located off-shore Pehuén-Co. The black diamond indicates the location where the validation between satellite and simulated significant wave height ( $H_s$ ) trends was carried out.

The coast of the Buenos Aires (Fig. 1) is constituted almost entirely of sandy beaches, with seaside resorts crowded with tourists in the summer. The only exceptions are Mar del Plata and some areas of Quequén and Necochea where the coast is constituted by cliffs. The mean wave height along the coast slightly increases south-westwards and ranges from 1 m to 1.5 m (Dragani et al., 2010). The tide regime is mixed, predominantly semidiurnal (Balay, 1955) and the tidal range increases westwards (SHN, 2017), from Mar del Plata (0.83 m) to Bahía Blanca (2.62 m). Some particular beach resorts located along the southern coast of Buenos Aires

(Fig.1) are incurring natural erosive processes, which are aggravated by human activities including urbanization, foredune degradation and/or sand mining. In this regard, some authors reported an increase in the erosive processes along the coast of Buenos Aires during the last three decades of the 20th century. For instance, Kokot (1997) linked together the enhanced erosion with changes in atmospheric and oceanic processes which seem to be a consequence of climate change. The erosion process along the coast of Buenos Aires was also studied by Diez et al. (2007), who related it to increased sea level. Some particular areas of the southern coast of Buenos Aires are significantly affected by cliff erosion. Regarding this matter, Isla and Cortizo (2014) estimated a mean rate of cliff retreat of about 0.5/0.6 m/year, by comparing old photographs with modern satellite images. Moreover, a study of morphological changes along the coastline of Necochea and Quequén was carried out by Merlotto et al. (2013) through the analysis of aerial photographs, satellite images, and beach profiles. Even though some evidences of beach stability were observed at Necochea, the retreat of the coastline and a negative sedimentary balance at Quequén could indicate an accentuated erosion process. Furthermore, evident and progressive coastal changes produced by erosion are clear for the neighborhoods of Pehuén-Co and Monte Hermoso. These alterations are causing private capital losses and risks in nature and anthropologic reserves (Rojas et al., 2014).

Variation in wave climate could be the trigger of alterations in the littoral processes of the region. For this reason, Dragani et al. (2013) studied the wave climate employing numerical simulation with the SWAN model, along the northern coast of Buenos Aires. They found a significant increase of wave heights (S and SSE directions). Furthermore, this simulation presented an increase in the number of cases of waves coming from the S, SSE, and E.

Additionally, the area located between Pehuén-Co and Monte Hermoso has been designated as a geological, paleontological and archaeological reserve and it may be declared a World Heritage Site by UNESCO. This region in particular constitutes a worldwide unique system

237  
238  
239 due to the existence of anthropological and paleontological footprints (Perillo and Iribarne,  
240  
241 2003).

242  
243  
244  
245  
246 Despite the importance of the understanding of wave climate, its changes and impacts on the  
247  
248 coast and its associated longshore energy flux, there are almost no systematic measurements of  
249  
250 wind wave parameters between Bahía Blanca and Mar del Plata. There are only two relatively  
251  
252 short wave data records: the first wave data series is currently being collected (since 2007, with  
253  
254 a non-directional wave sensor) 21 km off-shore Pehuén-Co (Fig. 1). And the second wave data  
255  
256 series were measured 500 m off-shore Quequén Port with a S4 Interocean current/wave meter.  
257  
258 This last data record began in 2007 and presents several gaps, some of them significantly long.  
259  
260 The lack of long-term, systematic and directional wave data series explains, in part, the scarce  
261  
262 amount of scientific papers about longshore currents, near shore circulation, onshore/off-shore  
263  
264 and longshore sediment transport (and their time and space variability) along the southern coast  
265  
266 of Buenos Aires.  
267  
268  
269  
270

271  
272 Perhaps the largest impact on coastal stability is caused by the variability or change of the  
273  
274 longshore net sediment transport (Syvitski et al., 2005). It is assumed that the net transport of  
275  
276 sand in the southern coast of Buenos Aires, between the estuary of Bahia Blanca and Mar del  
277  
278 Plata, is predominantly from SW to NE (Perillo et al., 2005). This assumption is mainly  
279  
280 supported by the progressive accumulation of sand observed on the western side of the western  
281  
282 breakwater of Quequén Port. Nevertheless, the prevailing direction of the net sand transport is  
283  
284 rather uncertain between Bahia Blanca estuary and Quequén Port. The absence of coastal  
285  
286 structures along this coastal area – which usually provides a clear indication of the prevailing  
287  
288 direction of the net transport – contributes to maintaining this uncertainty. However, it is  
289  
290 largely known that the potential longshore sediment transport rate can be estimated from the  
291  
292  
293  
294  
295

296  
297  
298 longshore component of the wave energy flux in the surf zone (CERC, 1984). Therefore, the  
299  
300 main objective of this work is to carry out an integral study of the longshore wave energy flux  
301  
302 along the southern coast of Buenos Aires, between Bahia Blanca and Mar del Plata (Fig. 1).  
303  
304 Long-term data series of wave parameters were simulated using SWAN (Simulated Waves  
305  
306 Nearshore) model for the period 1979-2012. In addition, satellite data have not enough  
307  
308 time/space resolution and are rather short for carrying out climatic studies. Annual longshore  
309  
310 energy flux, (space and time) variability and trends were computed from simulated wave  
311  
312 parameters at selected locations of the study area. The correlation between estimated annual  
313  
314 energy flux and some climatic indices, usually adopted to describe the ENSO (El Niño /  
315  
316 Southern Oscillation) and the SAM (Southern Annual Mode), are investigated and discussed  
317  
318 in this paper.  
319  
320

## 321 322 323 **2. Data and Methods**

### 324 325 326 327 **2.1. Wave Model**

328  
329  
330  
331  
332 Wave parameters, annual longshore energy flux, and trends were derived from numerical  
333  
334 simulations carried out with the SWAN model. This is a numerical wave model that provides  
335  
336 realistic estimates of wave parameters in coastal areas (Booij et al., 1999; Ris et al., 1999;  
337  
338 Holthuijsen et al., 2004). The implementation of the model to the study region spans the area  
339  
340 between 38° S and 42.5° S, and 58° W and 66° W, with a grid space resolution of 7 km × 7 km  
341  
342 (75 × 96 grid points). The model domain is presented in Figure 2. The boundary conditions  
343  
344 were provided by a larger low resolution grid covering the area between 31° S and 47° S, and  
345  
346 45° W and 68° W, with a grid space resolution of 23 km x 23 km (77 x 87 grid points). It has  
347  
348  
349  
350  
351  
352  
353  
354



355  
356  
357 been demonstrated (Dragani et al., 2008) that this extended domain is large enough to generate  
358  
359 realistic wind wave fields (sea and swell) in the Buenos Aires coastal area.  
360  
361

362  
363  
364 The atmospheric forcing were the four daily fields (0, 6, 12 and, 18 GMT) of the 10 m wind  
365  
366 components from the NCEP/NCAR Reanalysis I. This reanalysis has been successfully  
367  
368 implemented as forcing in several numerical regional studies in the area (Simionato et al., 2005,  
369  
370 2006a, b, 2007; Dragani et al., 2010; Codignotto et al., 2012). A discussion about the quality  
371  
372 of NCEP/NCAR I over the Southern Hemisphere can be found in Simmonds and Keay (2000),  
373  
374 and a complete description of this reanalysis and its dataset can be found in Kalnay et al. (1996).  
375  
376 Recently Pescio et al. (2016) showed that, even though the Climate Forecast System Reanalysis  
377  
378 (CFSR) is a newer reanalysis with higher time and space resolution executed in a coupled  
379  
380 mode, wind speed trends seem to be better reflected by the NCEP/NCAR I in the study area.  
381  
382

383  
384  
385 The model was run in a non-stationary mode, whereas the bathymetry was obtained as a  
386  
387 combination of a depth dataset (space resolution:  $0.0167^0 \times 0.0167^0$ ) obtained from GEBCO  
388  
389 (2003) for deep waters (>200 m) and digitized nautical charts for the continental shelf (SHN,  
390  
391 1986, 1992, 1993, 1999a, b). The drag coefficient was modified according to Simionato et al.  
392  
393 (2006) and Dragani et al. (2008).  
394  
395  
396  
397  
398  
399  
400  
401  
402  
403  
404  
405  
406  
407  
408  
409  
410  
411  
412  
413

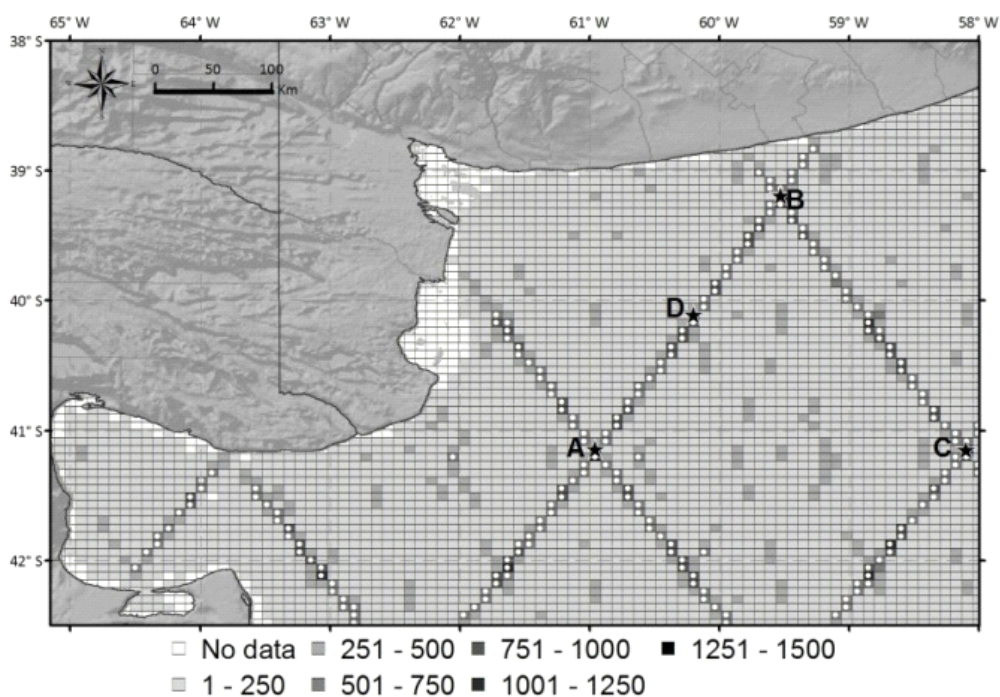
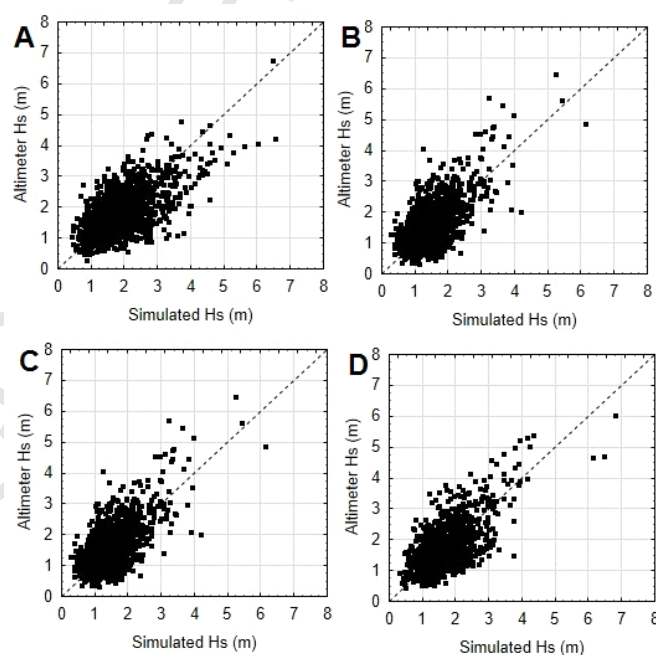


**Figure 2.** High resolution model domain. The available amount of altimeter data (period: 1991 – 2012) is denoted for each grid cell. White circles indicate locations where simulated Hs were validated. Points A, B, C and D indicate locations where scatter plots between satellite data and simulated Hs are shown (see Fig. 3).

Numerical simulations were validated using in situ and satellite wave parameters. Firstly, modeled significant wave heights (Hs) were compared with altimeter Hs data available in the study area. The altimeter database was obtained from the Globwave Project (Queffeuilou and Croizé-Fillon, 2013) and consists on calibrated Hs from eight missions: ERS-1, ERS-2, TOPEX-Poseidon, GEOSAT Follow-ON (GFO), Jason-1, Jason-2, ENVISAT and CryoSat, covering the 1991-2012 period. Altimeter data were gridded in order to match them to the implemented high resolution model grid. The available amount of satellite measurements corresponding to each grid cell is presented in Fig. 2. As it can be seen in that figure, the majority of the grid cells in the computational domain have very few altimeter data (less than 250 data) to carry out a satisfactory validation. Only grid cells with more than 750 altimeter data were considered. Then, approximately 200 grid cells were selected to perform the validation of the numerical simulations which are indicated with white circles in Fig. 2. Scatter

plots between satellite and simulated Hs show a good agreement for the study region. Mean bias (measured Hs minus modeled Hs) resulted equal to 0.04 m, mean scatter index (root mean square error to mean measured Hs ratio) was 0.37 and mean correlation index was 0.61. Scatter plots for the four grid cells with more altimeter data (namely A, B, C, and D in Fig. 2) are presented in Fig. 3. On the other hand, simulated Hs were compared with observed Hs measured near Bahía Blanca (Fig. 1) in the period 2007 - 2011. This period was selected because it presents a minimal amount of gaps. The resulting bias (0.11 m), scatter index (0.52) and correlation index (0.55) indicated a good performance of the numerical simulations. Wave data gathered near the mouth of Quequén Port were not used for validation because they were obtained very close to the coast. In addition trends in simulated wave parameters were also validated against altimeter wave height data trends for the period 1992 - 2012. Trends for altimeter data and modeled wave heights are presented for the node B (Fig. 2) which is the node closest to the coast in the study region. As a result, computed trends were very similar: +7.3 mm/decade for modeled wave heights and +7.7 mm/decade for altimeter wave parameters.



532  
533  
534 **Figure 3.** Scatter plots between satellite and simulated Hs for selected grid cells. Locations are indicated with  
535  
536 points A, B, C and D in Fig. 2.  
537

## 538 539 **2.2 Longshore wave energy flux**

540  
541  
542  
543  
544 The statement that the prevailing direction of the net sand littoral transport is eastwards at  
545  
546 Quequén, with a maximum estimated value of  $1.3 \cdot 10^6 \text{ m}^3 \text{ yr}^{-1}$ , is supported by few observations  
547  
548 (Framiñan, 1990). Nevertheless, there is some uncertainty about the predominant direction of  
549  
550 the littoral transport in the coastal area located at the west of Quequén, between Monte  
551  
552 Hermoso and Bahía Blanca. The potential longshore sediment transport can be considered  
553  
554 proportional to the longshore wave energy flux per unit crest (PI) given by:  
555  
556

$$557 \text{PI} = 0.05 \rho g^{3/2} H_s^{5/2} (\cos \alpha)^{1/4} (\sin 2\alpha) \quad (1)$$

558  
559  
560  
561  
562 which was recommended by CERC (1984). In this expression  $\rho$  is the density of seawater  
563  
564 (constant, equal to  $1030 \text{ kg m}^{-3}$ ),  $g$  the acceleration due to gravity ( $9.86 \text{ m s}^{-2}$ ),  $H_s$  the significant  
565  
566 wave height and  $\alpha$  the wave angle between the wave crest and the shoreline, both wave  
567  
568 parameters corresponding to deep waters. The predominant orientation of the shoreline was  
569  
570 estimated from Landsat images (Data SIO, NOAA, U.S. Navy, NGA, GEBCO, source: Google  
571  
572 Earth, 2016). The orientation of the shoreline (respect to a geographic parallel) ranges from  $0^\circ$   
573  
574 (W-E) on the west area of the study region to  $33^\circ$  (SW-NE) on the east area. Computed PI can  
575  
576 be positive (eastward) or negative (westward) depending on the instantaneous value of  $\alpha$ .  
577  
578 Accordingly, annual net PI ( $\text{PI}_N$ , the sum of the individual PI in a year) can also result in an  
579  
580 eastward direction (positive) or a westward direction (negative). Annual western PI ( $\text{PI}_W$ , the  
581  
582 sum of the negative PI in a year) and annual eastern PI ( $\text{PI}_E$ , the sum of the positive PI in a year)  
583  
584 were also obtained.  
585  
586  
587  
588  
589  
590

### 3. Results

Simulated Hs (period: 1979-2012) were analyzed for thirteen selected locations placed between Pehuén-Co and Mar del Sur (Fig. 1). Mean Hs increases eastwards, from 0.60 to 1.20 m, and maximum Hs also increases eastwards reaching values up to 6.3 m close to Mar del Sur. Waves predominantly propagate northwards in this region (25% of cases). Trends in wind wave heights were analyzed in the study area. Significant positive trends were detected near Mar del Plata (points: 11, 12 and 13) reaching maximum values of +16 mm/decade. In addition, trends in wave heights (Hs) were also studied considering the eight main directions (N: for waves coming between  $337.5^\circ$  and  $22.5^\circ$ , NE: between  $22.5^\circ$  and  $67.5^\circ$ , E: between  $67.5^\circ$  and  $112.5^\circ$ , and so on). Trends in Hs were statistically different from zero only for the E and NE directions. Computed trends, for waves coming from the E and NE, are ranged from +8 and +23 mm/decade and from +8 and +31 mm/decade, respectively. In order to illustrate these trends, simulated mean annual Hs and fitted regression lines (which show the mean trends) for waves coming from the E and NE, for locations 1 and 9, are presented in Fig. 4. Mean annual Hs and fitted regression lines corresponding to other locations are similar to them and are not included in this work. Computed trends for directional frequency of occurrence (number of cases per year, for the eight directions) were also studied. Negative trends (significantly different from zero, with 95 % confidence) were obtained for waves coming from the SW for all analyzed locations. Negative trends were also obtained for waves propagating from the NW, but they were slightly smaller than trends for waves propagating from SW and are only significantly different from zero at locations 11, 12 and 13.

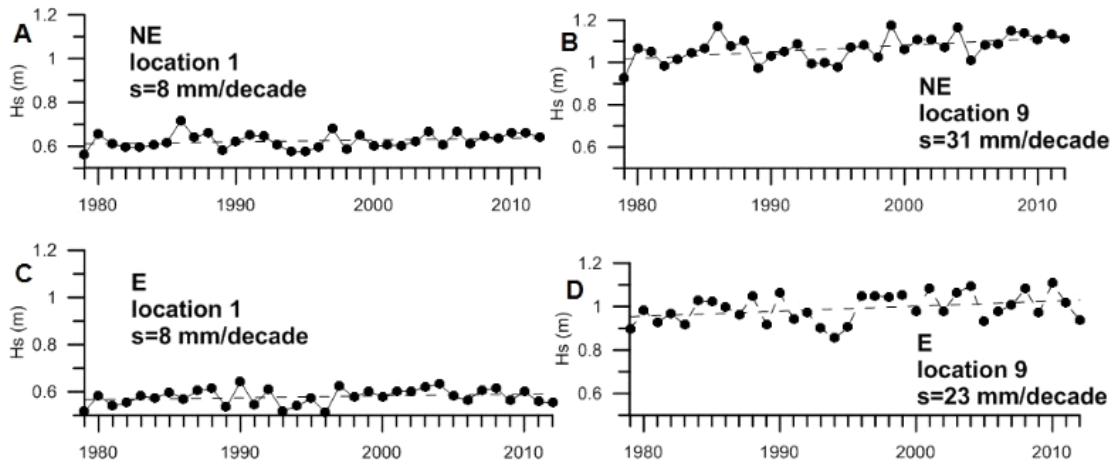


**Figure 4.** Mean annual Hs (period: 1979-2012) for waves coming from NE (A-B) and E (C-D) for point 1 (A-C) and point 9 (B-D). Least-square regression (dashed) line and trends (mm/decade) are also included.

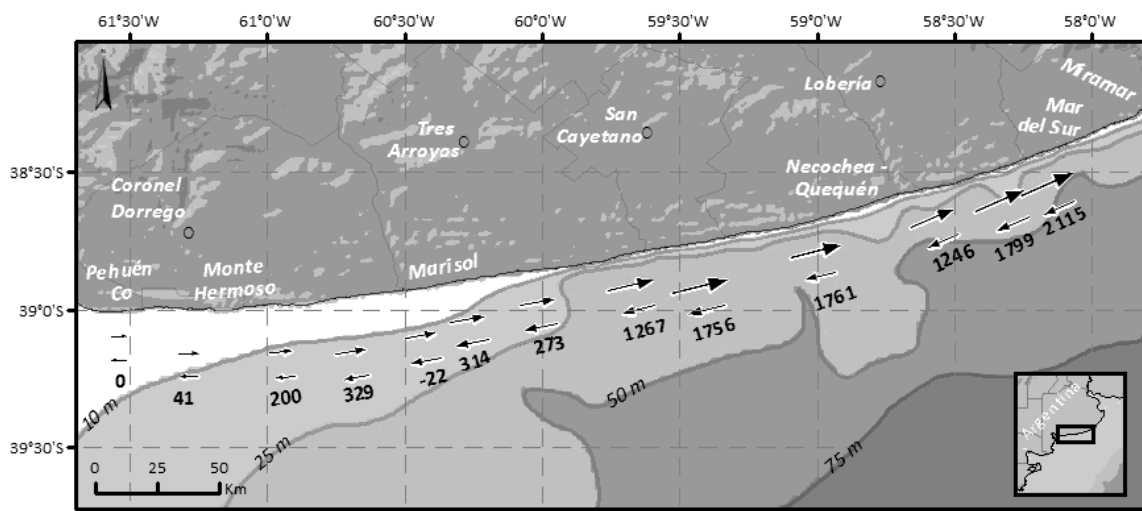


**Figure 5.** Averaged annual westward and eastward PI (period: 1979-2012) are indicated with arrows. Values of  $PI_{N-AVE}$  are also presented (in  $J m^{-1} s^{-1}$ ), positive values correspond to eastward  $PI_{N-AVE}$ .

Average  $PI_N$  were calculated for the period 1979-2012 ( $PI_{N-AVE}$ ) which resulted in a predominantly eastward direction (Fig. 5). Subsequently, this last fact supports that the annual rate of the potential longshore transport would be mainly eastwards between Bahía Blanca and Mar del Plata.  $PI_{N-AVE}$  increases eastwards, from a null value at location 1 to a maximum value

(2150 J m<sup>-1</sup>s<sup>-1</sup>) at location 13.  $PI_{N-AVE}$  was virtually negligible (not statistically different from zero) at sites 2 and 5, located in the western zone of the study region. Westward and eastward averaged PI ( $PI_{W-AVE}$  and  $PI_{E-AVE}$ , respectively) were also computed for the period 1979-2012.  $PI_{W-AVE}$  and  $PI_{E-AVE}$  are represented with arrows and the values (in J m<sup>-1</sup>s<sup>-1</sup>) of  $PI_{N-AVE}$  are included in Fig. 5. In the western zone,  $PI_{N-AVE}$  is one or two orders of magnitude smaller than the values corresponding to the eastern zone, where  $PI_{N-AVE}$  is towards the E. Consequently, taking into account the computed values of  $PI_{N-AVE}$ , the thirteen locations analyzed were preliminarily clustered in two different groups: the western (locations 1 to 7) and eastern groups (locations 8 to 13). The western locations presented relatively low values of  $PI_{N-AVE}$  (160 J m<sup>-1</sup>s<sup>-1</sup>) while the eastern locations showed values approximately ten times greater (1650 J m<sup>-1</sup>s<sup>-1</sup>). Values of  $PI_N$  are presented for each location in Fig. 6. Averaged  $PI_N$  for the western group of locations (1 to 7, black line) and for the eastern group (8 to 13, grey line) are also shown in Fig. 6. It can be noted that differences between western and eastern  $PI_N$  are minimal for the years 1983, 1998 and 2001. This issue will be particularly discussed in the next section. A linear fit was carried out between pairs of western and eastern averaged  $PI_N$  corresponding to the period 1979-2012.  $PI_N$  for the years 1983, 1998 and 2001 were excluded from this analysis because they were considered atypical. The computed slope of the linear fit was equal to 0.14. This stated that the western averaged  $PI_N$  is approximately 14% of the eastern averaged  $PI_N$ .  $PI_N$  and  $PI_E$  data series do not present significant trends in the study region (locations 1 to 13, period: 1979-2012). In contrast,  $PI_W$  data series showed significant negative trends at locations 3 to 6, which ranged from -30 to -70 Jm<sup>-1</sup>s<sup>-1</sup>/decade.

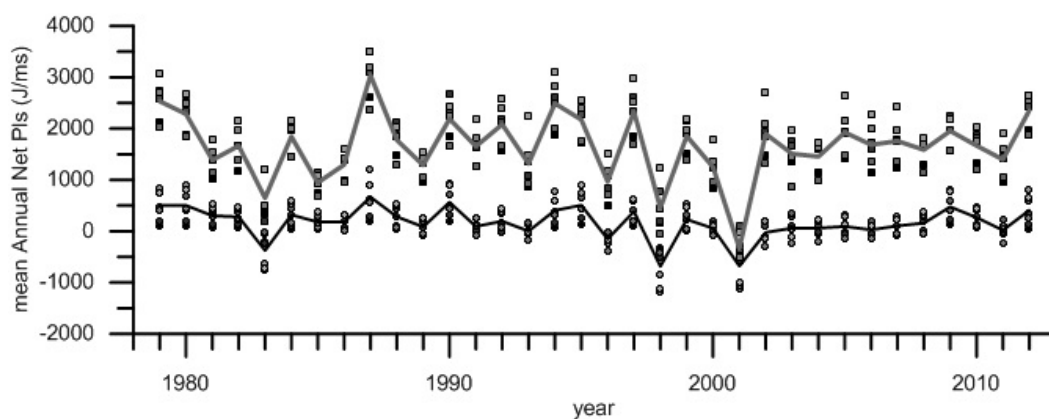


**Figure 6.**  $Pl_N$  data series for thirteen analyzed locations (period 1979 – 2012). Averaged  $Pl_N$  for locations clustered in the western group (locations 1 to 7, black line) and in the eastern group (locations 8 to 13, grey line) are also included.

Standard deviations of  $Pl_N$  data series ( $SD_{PLN}$ ) were computed for every location. The eastern group of locations presented  $SD_{PLN}$  twice as large as the values assessed for the western group (650 and 300  $Jm^{-1}s^{-1}$ , respectively). In addition, correlation coefficients were computed for all possible pair combinations of  $Pl_N$  data series corresponding to the thirteen locations of the study area. Then, 78 correlation coefficients ( $r_{i-j}$ ) were obtained, where  $r_{i-j}$  is the correlation coefficient computed between data series corresponding to locations  $i$  and  $j$  ( $1 \leq i \leq 13$ ,  $1 \leq j \leq 13$ ,  $i \neq j$  and  $r_{i-j} = r_{j-i}$ ). All correlation coefficients were significantly different from zero and inversely proportional to the distance between different locations. Correlation coefficients for western locations (1 to 7) ranged from 0.86 to 0.99 and for the eastern locations (8 to 13) from 0.85 to 0.99. The lowest coefficient was obtained for correlation computed between locations 2 and 13 ( $r_{2-13} = 0.51$ ). Then, even though  $Pl_N$  data series can be clustered into two defined groups, all of them (locations 1 to 13) presented fairly similar inter-annual variability.



#### 4. Discussion

Annual net longshore energy flux and its (space and time) variability and trends were inferred from long-term numerical simulations carried out with the validated SWAN model at the southern coast of Buenos Aires. It is important to highlight that there are not regional antecedents in the peer reviewed scientific literature about this subject. Numerical simulations carried out in this work have shown that the wave climate is significantly different between the northern and southern coast of Buenos Aires. The most frequent wave direction is from the S (around 25 % of cases) in the southern coast of Buenos Aires. But, wave direction in the Río de la Plata mouth, located approximately 600 km north-eastwards from the study area, is rather different: from the SE (41%), E (28%) and S (14%) (Dragani and Romero, 2004). In addition, significant positive wave height trends, for the E and NE directions, and significant negative trends in the frequency of occurrence, only for the SW direction, were found on the southern coast of Buenos Aires.

$PI_N$  were calculated from simulated wave parameters for the period 1979-2012. Predominant eastward values of  $PI_{N-AVE}$  were obtained and, consequently, the rate of the potential sediment transport would be also positive (eastwards) and would increase towards the E. This fact is consistent with some visual evidences of accumulation of sand (for example, at Quequén Port) and with some preliminary studies carried out at Mar del Plata, located approximately 200 km east-northeastwards from Quequén. For example, Caviglia (1991) estimated a north-eastward sediment transport rate ranged from  $0.3$  to  $1.0 \times 10^6 \text{ m}^3 \text{ yr}^{-1}$  at Mar del Plata. More recently, Dragani et al. (2013) inferred a north-northeastward direction and negative trends (approximately -20% per decade) for  $PI_N$  at Pinamar, located around 100 km north-eastward Mar del Plata. On the contrary, no significant trend for  $PI_N$  and  $PI_E$  were inferred in the southern

886  
887  
888 coast of Buenos Aires. However slight but significant negative trends for  $PI_W$  (-2.5% per  
889 decade) were obtained at locations 3 to 7 placed in the western zone of the study area.  
890  
891

892  
893  
894  $PI_{N-AVE}$  increases towards the E, but not regularly.  $PI_{N-AVE}$  increases abruptly from 273 to 1267  
895  $J\ m^{-1}s^{-1}$  from location 7 to 8, that is, at the border between the western and eastern clusters.  
896  
897 Consequently, the rate of the potential longshore sediment transport would be significantly  
898 greater at location 8 than at location 7. The longshore sediment transport budget can be studied  
899 in a control volume defined between two transects normal to the coast in the surf zone. The on-  
900 shore/off-shore sediment transport is not taken into account in this preliminary analysis. For  
901 instance, if a control volume containing locations 7 and 8 is considered, the alongshore  
902 sediment budget will be negative and then the coast will be under an important erosive process.  
903  
904 Differential imbalances like these in the longshore sediment transport could be a reasonable  
905 and preliminary explanation for the reported natural erosion along the southern coast of Buenos  
906 Aires (Rojas et al., 2014). For instance, observational evidences show that Marisol (Fig. 5) is  
907 clearly an erosive beach. It could be explained because  $PI_{N-AVE}$  presents a noticeable divergence  
908 between locations 5 and 6, -22 and 314  $J\ m^{-1}s^{-1}$ , respectively. The alongshore sediment  
909 transport is westwards at location 5 and eastwards at 6 and consequently, the coast is under  
910 considerable erosive processes.  
911  
912  
913  
914  
915  
916  
917  
918  
919  
920  
921  
922  
923  
924  
925  
926  
927

928  
929 High inter-annual variability in  $PI_N$  data series, especially at points clustered at the eastern  
930 group, can be clearly appreciated in Fig. 6. Even though  $PI_N$  is usually positive, negative values  
931 can be observed for years 1983, 1998 y 2001. These anomalous values of  $PI_N$  are possibly  
932 associated with atypical values in wave directions. Unusually high frequencies of occurrence  
933 were found for waves coming from the SE in 1998 and 2001, which are directly associated to  
934 negative values of  $PI_N$ . These anomalous wave directions could probably be linked to regional  
935  
936  
937  
938  
939  
940  
941  
942  
943  
944

945  
946  
947 variability in the surface wind circulation. Thus, possible relationships between the inter-annual  
948  
949 variability in  $PI_N$  and two climatic indices were investigated.  
950

951  
952  
953 The ENSO (El Niño - Southern Oscillation) cycle refers to the coherent and sometimes very  
954 strong year-to-year variations in sea-surface temperatures, convective rainfall, surface air  
955 pressure and atmospheric circulation that occur across the equatorial Pacific Ocean  
956 ([http://www.cpc.noaa.gov/products/analysis\\_monitoring/ensostuff/ensofaq.shtml#NINO](http://www.cpc.noaa.gov/products/analysis_monitoring/ensostuff/ensofaq.shtml#NINO)). The  
957  
958 Climate Prediction Center (<http://www.cpc.noaa.gov>) reported that two of the more intense  
959  
960 ENSO events occurred in 1982-1983 and 1997-1998. Correlation coefficients between the  $PI_N$   
961  
962 data series and the Southern Oscillation Index (SOI) were calculated and showed significant  
963  
964 correlation (95% confidence level) for the easternmost locations of the study region (from 10  
965  
966 to 13). The maximum correlation coefficient was obtained at location 13 (0.52).  
967  
968  
969  
970  
971  
972  
973  
974

975 The SAM (Southern Annual Oscillation) is one of the annular modes of variability. It describes  
976  
977 the north-south movement of the westerly wind belt  
978  
979 (<http://www.bom.gov.au/climate/enso/history/ln-2010-12/SAM-what.shtml>). Correlation  
980  
981 coefficients between the  $PI_N$  data series and the SAM index were assessed and showed  
982  
983 significant correlation (95% confidence level) for the easternmost locations of the study region  
984  
985 (from 9 to 13). The maximum correlation coefficient was also obtained at the easternmost  
986  
987 location (0.53). A comparison between normalized energy flux series with SOI and SAM  
988  
989 indices are presented in Figures 7 and 8, respectively. Normalized  $PI_N$  series and SOI present a  
990  
991 good agreement. Some differences can be seen between 1979 and 1985 and between 1999 and  
992  
993 2001 (Fig. 7). Normalized  $PI_N$  series and SAM index also present a good agreement. The main  
994  
995 differences can be appreciated at the beginning of the period, between 1979 and 1983 (Fig. 8).  
996  
997  
998  
999  
1000  
1001  
1002  
1003

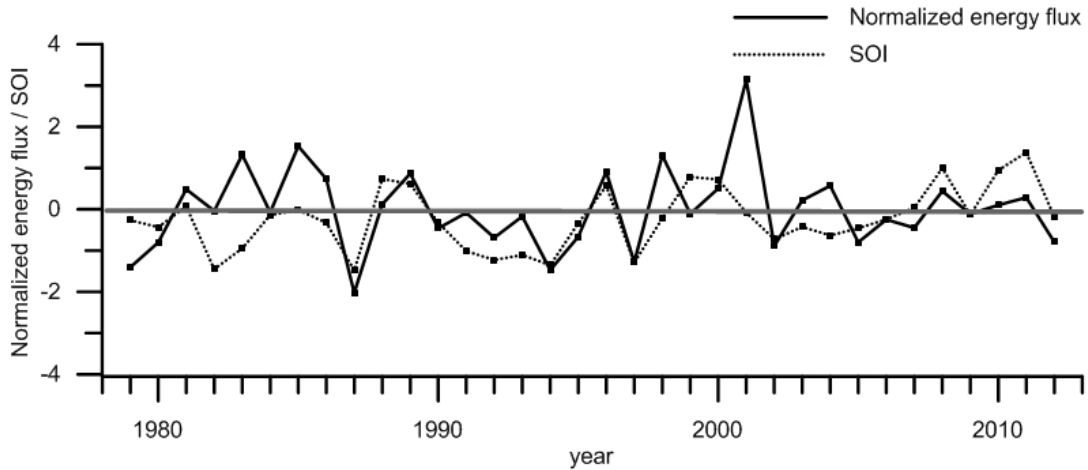


Figure 7. Normalized  $PI_N$  and SOI series for location 13.

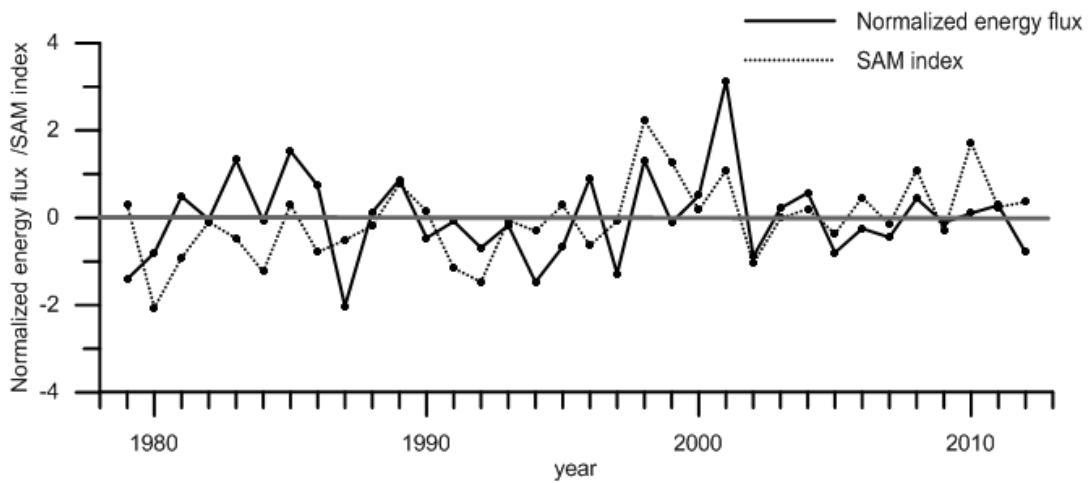


Figure 8. Normalized  $PI_N$  and SAM index series for location 13.

## 5. Conclusion

Space and time variability of the longshore energy flux, estimated from a validated wave numerical model (SWAN), was investigated along the southern coast of Buenos Aires. Results have shown that the wave climate along the southern coast of Buenos Aires is significantly different from the wave climate along the northern coast. The most frequent wave direction is northwards (around 25 % of the cases). Significant positive wave height trends (for E and NE directions) and significant negative trends in the frequency of occurrence (for SW direction) were found along the southern coast. Average  $PI_N$  is predominantly eastwards and increases

1063  
1064  
1065 from W to E in the study region (Fig. 5). Subsequently, the rate of the potential annual  
1066 longshore transport would be mainly eastwards between Bahía Blanca and Mar del Plata.  $PI_{N-AVE}$   
1067 and  $PI_N$  standard deviations computed from the data series located in the eastern zone are  
1068 significantly greater than values corresponding to data series in the western zone.  
1069 Consequently, the thirteen analyzed locations can be clustered in two groups: the western  
1070 (locations 1 to 7) and eastern groups (locations 8 to 13).  $PI_{N-AVE}$  increases abruptly from 273  
1071 to  $1267 \text{ J m}^{-1}\text{s}^{-1}$ , from location 7 to 8. Therefore, the rate of the potential longshore sediment  
1072 transport would be significantly greater at location 8 than at location 7. These imbalances in  
1073 the longshore sediment transport could be a reasonable and preliminary explanation for the  
1074 reported natural erosion along the southern coast of Buenos Aires.

1085  
1086  
1087 Correlation coefficients were computed for all possible pairs of combinations of  $PI_N$  data series  
1088 corresponding to the thirteen locations. All correlation coefficients were significantly different  
1089 from zero and inversely proportional to the distance between locations. Then, even though data  
1090 series of  $PI_N$  can be clustered into two defined groups, all of them seem to show fairly similar  
1091 inter-annual variability. High inter-annual variability in the  $PI_N$  data series can be noticed at  
1092 locations clustered in the eastern group (Fig. 6). Possible connections between the inter-annual  
1093 variability and climatic indices related to ENSO and SAM were investigated. Significant  
1094 correlation coefficients (greater than 0.5) were obtained for both indices at the easternmost  
1095 locations of the study region. This indicates that both climatic anomalies would impact on the  
1096 wave climate along the southern coast of Buenos Aires.

1097  
1098  
1099 **Acknowledgments:** This paper is a contribution to the CONICET PIP 112-201501-00174-CO  
1100 project.  
1101  
1102  
1103  
1104  
1105  
1106  
1107  
1108  
1109  
1110  
1111  
1112  
1113  
1114  
1115  
1116  
1117  
1118  
1119  
1120  
1121

## References

- Balay, M., 1955. La determinación del nivel medio del Mar Argentino, influencias de las oscilaciones del mar no causadas por la marea, Dir Gral de Nav. Hidrog, Min de Mar.
- Bertin, X., Prouteau, E., Letetrel, C., 2013. A significant increase in wave height in the North Atlantic Ocean over the 20th century. *Glob. Planet. Change* 106, 77–83. doi:10.1016/j.gloplacha.2013.03.009
- Booij, N., Ris, R.R.C., Holthuijsen, L.H.L., 1999. A third-generation wave model for coastal regions 1. Model description and validation. *J. Geophys. Res.* 104, 7649–7666. doi:10.1029/98jc02622
- Caviglia, F., Pousa, J., Lanfredi, N., 1991. A determination of the energy flux constant from dredge records. *J. Coast. Res.* 7, 543–549.
- CERC, 1984. Shore Protection Manual, Vol. 1. Coastal Engineering Research Center, Department of Army, US Army Corps of Engineers, Washington DC.
- Codignotto, J.O., Dragani, W.C., Martin, P.B., Simionato, C.G., Medina, R. A., Alonso, G., 2012. Wind-wave climate change and increasing erosion in the outer Río de la Plata, Argentina. *Cont. Shelf Res.* 38, 110–116. doi:10.1016/j.csr.2012.03.013.
- Dean, R., Dalrymple, R., 2002. Coastal Processes with Engineering Applications, Water. doi:10.2277/0521602750
- Delgado, A.L., Vitale, A.J., Perillo, G.M.E., Piccolo, M.C., 2012. Preliminary Analysis of Waves in the Coastal Zone of Monte Hermoso and Pehuén Co, Argentina. *J. Coast. Res.* 283, 843–852. doi:10.2112/JCOASTRES-D-10-00136.1
- Diez, P.G., Perillo, G.M.E., Piccolo, M.C., 2007. Vulnerability to Sea-Level Rise on the Coast of the Buenos Aires Province. *J. Coast. Res.* 231, 119–126. doi:10.2112/04-0205.1
- Dragani, W.C., Romero, S.I., 2004. Impact of a possible local wind change on the wave climate in the upper Río de la Plata. *Int. J. Climatol.* 24, 1149–1157. doi:10.1002/joc.1049
- Dragani, W.C., Garavento, E., Simionato, C.G., Nuñez, M.N., Martin, P., Campos, M.I., 2008. Wave Simulation in the Outer Río de la Plata Estuary : Evaluation of SWAN Model 299–305.
- Dragani, W.C., Martin, P.B., Simionato, C.G., Campos, M.I., 2010. Are wind wave heights increasing in south-eastern South American continental shelf between 32° S and 40° S? *Cont. Shelf Res.* 30, 481–490. doi:10.1016/j.csr.2010.01.002
- Dragani, W.C., Martin, P.B., Alonso, G., Codignotto, J.O., Prario, B.E., Bacino, G., 2013. Wind wave climate change: Impacts on the littoral processes at the Northern Buenos Aires Province Coast, Argentina. *Clim. Change* 121, 649–660. doi:10.1007/s10584-013-0928-8
- Framiñan M., 1990. Transporte de sedimentos en Pinamar, Provincia de Buenos Aires. II Jornadas de Oceanografía Física y XVI Reunión Científica de Geofísica y Geodesia de la Asociación Argentina de Geofísicos y Geodestas, 15 pp., Bahía Blanca.
- GEBCO, 2003. User guide to the centenary edition of the GEBCO Digital Atlas and its data sets. In: Jones, M.T. (Ed.), Natural Environment Research Council.
- Hemer, M. A., Fan, Y., Mori, N., Semedo, A., Wang, X.L., 2013. Projected changes in wave climate from a multi-model ensemble. *Nat. Clim. Chang.* 3, 471–476. doi:10.1038/nclimate1791

- 1181  
1182  
1183  
1184  
1185  
1186  
1187  
1188  
1189  
1190  
1191  
1192  
1193  
1194  
1195  
1196  
1197  
1198  
1199  
1200  
1201  
1202  
1203  
1204  
1205  
1206  
1207  
1208  
1209  
1210  
1211  
1212  
1213  
1214  
1215  
1216  
1217  
1218  
1219  
1220  
1221  
1222  
1223  
1224  
1225  
1226  
1227  
1228  
1229  
1230  
1231  
1232  
1233  
1234  
1235  
1236  
1237  
1238  
1239
- Holthuijsen, L., Booij, N., Ris, R.C., Haagsma, L.G., Kieftenurg, A.T.M.M., Kriezi, E.E., Zijlema, M., Van der Westhuysen, A.J., Padilla-Hernández, R., Rogers, E., Kaihatu, J., Petit, H., Campbell, T., Cazes, J., Hashimoto, N., 2004. Swan cycle III version 40.31, User Manual. Delft University of Technology, Faculty of Civil Engineering and Geosciences, Environmental Fluid Mechanics Section: Delft.
- Isla, F.I., Cortizo, L.C., 2014. Sediment input from fluvial sources and cliff erosion to the continental shelf of Argentina. *J. Integr. Coast. Zo. Manag. - Rev. Gestão Costeira Integr.* 14, 553–568. doi:10.5894/rgci472
- Izaguirre, C., Méndez, F.J., Espejo, A., Losada, I.J., Reguero, B.G., 2013. Extreme wave climate changes in Central-South America. *Clim. Change* 119, 277–290. doi:10.1007/s10584-013-0712-9
- Kalnay, E., Kanamitsu, M., Kistler, R., Collins, W., Deaven, D., Gandin, L., Iredell, M., Saha, S., White, G., Woollen, J., Zhu, Y., Chelliah, M., Ebisuzaki, W., Higgins, W., Janowiak, J., Mo, K.C., Ropelewski, C., Wang, J., Leetmaa, A., Reynolds, R., Jenne, R., Dennis, J., 1996. The NCEP/NCAR 40-Year Reanalysis Project. *Bull. Am. Meteorol. Soc.*
- Kokot, R.R., 1997. Littoral Drift, Evolution and Management in Punta Médanos, Argentina. *J. Coast. Res.* 20, 214–233.
- Merlotto, A., Bértola, G.R., Isla, F.I., Cortizo, L.C., Piccolo, M.C., 2013. Short and medium-term coastal evolution of Necochea Municipality, Buenos Aires province, Argentina. *Environ. Earth Sci.* 71, 1213–1225. doi:10.1007/s12665-013-2525-6
- Perillo, G.M.E., Iribarne, O.O., 2003. New mechanisms studied for creek formation in tidal flats: From crabs to tidal channels. *Eos, Trans. Am. Geophys. Union* 84, 1. doi:10.1029/2003EO010001
- Perillo, G.M.E., Pérez, D.E., Piccolo, M.C., Palma, E.D., Cuadrado, D.G., 2005. Geomorphologic and physical characteristics of a human impacted estuary: Quequén Grande River Estuary, Argentina. *Estuar. Coast. Shelf Sci.* 62, 301–312. doi:10.1016/j.eccs.2004.09.018
- Pescio, A.E., Martin, P.B., Dragani, W.C., 2016. Winds speed trends over the southwestern Atlantic Ocean, between 33° and 50°S. *Int. J. Climatol.* 36, 501–507. doi:10.1002/joc.4348.
- Queffeuou, P., and Croizé-Fillon, D. 2013. Global altimeter SWH data set - May 2013. Plouzané, Francia: Laboratoire d'Océanographie Spatiale, IFREMER.
- Reguero, B.G., Méndez, F.J., Losada, I.J., 2013. Variability of multivariate wave climate in Latin America and the Caribbean. *Glob. Planet. Change* 100, 70–84. doi:10.1016/j.gloplacha.2012.09.005
- Ris, R.C., Holthuijsen, L.H., Booij, N., 1999. A third-generation wave model for coastal regions 2. Verification. *J. Geophys. Res.* 104, 7667–7681.
- Rojas, M.L., Recalde, M.Y., London, S., Perillo, G.M.E., Zilio, M.I., Piccolo, M.C., 2014. Behind the increasing erosion problem: The role of local institutions and social capital on coastal management in Argentina. *Ocean Coast. Manag.* 93, 76–87. doi:10.1016/j.ocecoaman.2014.03.010
- Simionato, C.G., Vera, C.S., Siegismund, F., 2005. Surface wind variability on seasonal and interannual scales over Río de la Plata area. *J. Coast. Res.* 21, 770–783. doi:10.2112/008-NIS.1

- 1240  
1241  
1242  
1243  
1244  
1245  
1246  
1247  
1248  
1249  
1250  
1251  
1252  
1253  
1254  
1255  
1256  
1257  
1258  
1259  
1260  
1261  
1262  
1263  
1264  
1265  
1266  
1267  
1268  
1269  
1270  
1271  
1272  
1273  
1274  
1275  
1276  
1277  
1278  
1279  
1280  
1281  
1282  
1283  
1284  
1285  
1286  
1287  
1288  
1289  
1290  
1291  
1292  
1293  
1294  
1295  
1296  
1297  
1298
- Simionato, C.G., Meccia, V.L., Dragani, W.C., Nuñez, M.N., 2006a. On the use of the NCEP/NCAR surface winds for modeling barotropic circulation in the Río de la Plata Estuary. *Estuar. Coast. Shelf Sci.* 70, 195–206. doi:10.1016/j.ecss.2006.05.047
- Simionato, C.G., Meccia, V.L., Dragani, W.C., Guerrero, R., Nuñez, M., 2006b. Río de la Plata estuary response to wind variability in synoptic to intraseasonal scales: Barotropic response. *J. Geophys. Res. Ocean.* 111, 1–14. doi:10.1029/2005JC003297
- Simionato, C.G., Meccia, V.L., Guerrero, R., Dragani, W.C., Nuñez, M., 2007. Río de la Plata estuary response to wind variability in synoptic to intraseasonal scales: 2. Currents' vertical structure and its implications for the salt wedge structure. *J. Geophys. Res. Ocean.* 112, 1–15. doi:10.1029/2006JC003815
- Simmonds, I., Keay, K., 2000. Mean southern hemisphere extratropical cyclone behavior in the 40-year NCEP-NCAR reanalysis. *J. Clim.* 13, 873–885. doi:10.1175/1520-0442(2000)013<0873:MSHECB>2.0.CO;2
- SHN, 1986. Mar Argentino, de Río de la Plata al Cabo de Hornos. Nautical Chart 50, 4th ed. Servicio de Hidrografía Naval, Buenos Aires, Argentina.
- SHN, 1992. Acceso al Río de la Plata. Nautical Chart H1, fifth ed. Servicio de Hidrografía Naval, Buenos Aires.
- SHN, 1993. El Rincón, Golfo San Matías y Nuevo. Nautical Chart H2, fourth ed. Servicio de Hidrografía Naval, Buenos Aires.
- SHN, 1999 a. Río de la Plata Medio y Superior. Nautical Chart H116, fourth ed. Servicio de Hidrografía Naval, Buenos Aires.
- SHN, 1999b. Río de la Plata Exterior. Nautical Chart H113, second ed. Servicio de Hidrografía Naval, Buenos Aires.
- SHN, 2017. Tablas de Marea. Publicación H-610, Servicio de Hidrografía Naval, Buenos Aires.
- Syvitski, J.P.M., Harvey, N., Wolanski, E., Burnett, W.C., Perillo, G.M.E., Gornitz, V., Arthurton, C.R.K., Bokuniewicz, H., Campbell, J.W., Cooper, L., Dunton, K., Gao, S., Hesp, P.P., Saito, Y., Salisbury, J., Snoussi, M., Yim, W.W., 2005. Chapter 2 Dynamics of the Coastal Zone. *Coast. Chang. Anthr.* doi:10.1007/3-540-27851-6
- Young, I.R., Babanin, A. V., Zieger, S., 2011. Global trends in wind speed and wave height. *Science* 332, 451–5. doi:10.1126/science.1197219